Magnesium Technology 2013
Edited by: Norbert Hort, Suveen N. Mathaudhu, Neale R. Neelameggham, and Martyn Alderman
TMS (The Minerals, Metals & Materials Society), 2013

THE INFLUENCE OF DEFORMATION MECHANISMS ON RUPTURE OF AZ31B MAGNESIUM ALLOY SHEET AT ELEVATED TEMPERATURES

Aravindha R. Antoniswamy[1], Alexander J. Carpenter[2], Jon T. Carter[3], Louis G. Hector, Jr.[3], and Eric M. Taleff[1, 2]
[1]The University of Texas at Austin; Materials Science and Engineering; 1 University Station C2200; Austin, TX 78712-0292, USA
[2]The University of Texas at Austin; Mechanical Engineering; 1 University Station C2200; Austin, TX 78712-0292, USA
[3]General Motors Research and Development Center; 30500 Mound Rd.; Warren, MI 48090-9055, USA

Keywords: AZ31B, bulge forming, rupture, deformation mechanism, cavity interlinkage, necking, anisotropy

Abstract

Gas-pressure bulge tests were conducted on Mg alloy AZ31B wrought sheet until rupture at temperatures from 250 to 450°C. The rupture orientation was observed to change with forming pressure, which controls the forming strain rate, at 350 to 450°C. This phenomenon is a result of associated changes in the mechanisms of plastic deformation. At slow strain rates ($\leq 3\times10^{-2}$ s^{-1}), cavity interlinkage associated with grain boundary sliding (GBS) creep induced rupture along the sheet rolling direction (RD). At fast strain rates ($\geq 3\times10^{-2}$ s^{-1}), flow localization (necking) associated with dislocation-climb-controlled (DC) creep induced rupture along the long-transverse direction (LTD), a result of mild planar anisotropy. Biaxial bulge specimens tested at 250 to 300°C ruptured explosively, hence preventing any further analysis.

Introduction

Wrought magnesium alloy sheets have high strength- and stiffness-to-weight-ratios compared to traditional steel and aluminum alloys [1]. Increased use of Mg can provide a significant reduction in the overall mass of a vehicle [2]. Vehicle light-weighting offers several performance advantages, which include improved fuel economy and reduced greenhouse gas emissions [3-6]. The extended range facilitated by the use of lightweight materials, such as Mg, is also beneficial for vehicles with alternative propulsion systems based upon fuel cells or batteries, for example.

Because of limited room-temperature ductility, forming of magnesium alloy sheet at elevated temperatures, where ductility is quite high, is of interest. Potential commercial hot-forming processes include gas-pressure forming, such as with superplastic forming and quick-plastic forming techniques [7, 8], and hot-die stamping. This study is primarily interested with the former. For gas-pressure forming, a sheet metal blank is clamped between two hot dies, and the sheet is formed into a cavity in one die using gas pressure [9]. The performance of a sheet material in such a forming process can be studied in the laboratory using the gas-pressure bulge test, for which the sheet is formed into an open cylindrical cavity. The stress states that occur in the sheet during gas-pressure bulge tests are characteristic of those that occur during hot gas-pressure forming of automotive components in manufacturing practice [10]. The die geometry in these tests can be tailored to form the sheet along a chosen strain path. For example, a cylindrical die is used to produce balanced biaxial tension at the bulge apex. Biaxial bulge testing is one type of test that can be used in constructing forming limit diagrams (FLDs). These tests can produce a nearly constant strain rate at the dome pole while avoiding any significant frictional effects, as the forming bulge does not contact the die cavity wall beyond a region of relief near the sealing bead [11]. Carpenter et.al. used biaxial bulge forming experiments to validate physics-based material models that predict the forming of AZ31B sheet at 450°C [12].

Cavity interlinkage and necking are the two mechanisms that control rupture in uniaxial tension tests of AZ31B sheet at elevated temperatures [13]. At 350 to 450°C, AZ31B deforms primarily by grain boundary sliding (GBS) creep at slow strain rates and by five-power dislocation-climb (DC) creep at fast strain rates [14]. Cavity interlinkage is associated with GBS creep [15] and, necking is associated with DC creep in AZ31B sheet.

The rupture behavior during biaxial bulge testing of AZ31B at 250 to 450°C is analyzed in this study. Metallography and EBSD studies are used to relate the change in rupture direction from along the sheet rolling direction (RD) to the sheet transverse direction (LTD) at 350 to 450°C to the underlying physics of deformation.

Experimental Procedure

Material

The material of this investigation is a 2-mm-thick AZ31B rolled alloy sheet supplied in the H24 temper [16]. The as-received microstructure is highly deformed, as shown in Figure 1. Hence, the average grain size could not be measured in the as-received condition. The composition of the alloy, as provided by the supplier, is given in Table I.

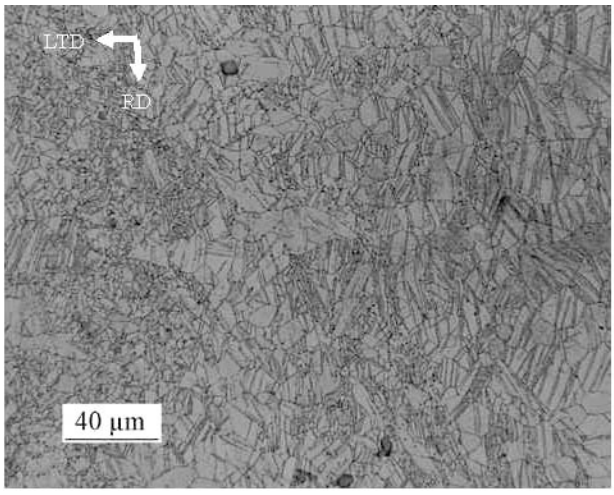

Figure 1. The as-received microstructure of AZ31B.

Table I. Composition of the AZ31B sheet material in wt. pct.

Al	Zn	Mn	Fe	Cu	Ni
3.1	1.0	0.42	0.006	0.003	<0.003
Si	**Ca**	**Be**	**Sr**	**Ce**	**Mg**
<0.1	<0.01	<0.005	<0.005	<0.01	Bal.

Gas-Pressure Biaxial Bulge Testing

Gas-pressure biaxial bulge testing was conducted using a custom instrument. This instrument forms a sheet blank at elevated temperature by gas pressure into an open cylindrical die with a 100-mm inner diameter to produce dome shapes. The dome pole experiences approximately balanced-biaxial tension. The stress state gradually changes down the slope of the dome toward the sealing bead, where a nearly plane-strain state exists. Prior to testing, a convective furnace heats the die set to the desired test temperature. A K-type thermocouple attached to each die monitors temperature. Once the dies reach the desired temperature, an AZ31B sheet blank is inserted, and the dies are then clamped together to form a sealing bead with the blank. The blank is held in the dies for a time sufficient to reach the desired test temperature. A prescribed gas pressure is then applied to form the blank into the die cavity. All tests were conducted until rupture, as determined by the leakage of gas pressure, as in Ref [11]. Figure 2 shows (a) the die setup used for biaxial bulge testing and (b) a tested specimen. Rupture typically occurred at the dome pole of the biaxial bulge specimens. Thickness strains were measured near the rupture. Average true-strain rates were then calculated by dividing rupture time into true strain near rupture. After rupture, the die halves are unclamped and the specimen is removed from the apparatus and allowed to air cool.

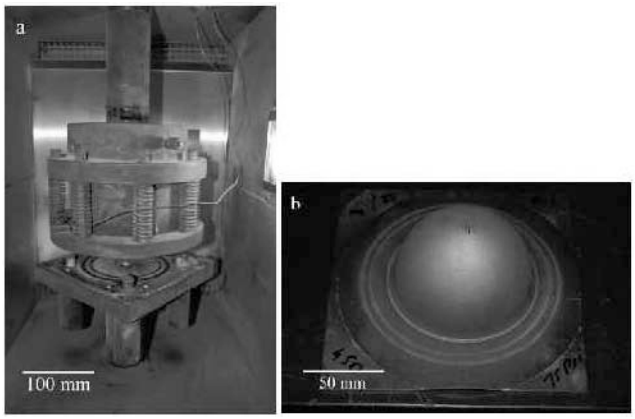

Figure 2. (a) The biaxial bulge testing dies and (b) a tested specimen are shown

Metallography

In order to examine the cross-section near rupture, tested biaxial bulge domes were sectioned perpendicular to the rupture orientation, and the sections were mounted in epoxy for metallographic examination. A specimen that ruptured along the RD was mounted to view the LTD-Short transverse direction (STD) plane, and a specimen that ruptured along LTD was mounted to view the RD-STD plane. All specimens were ground, polished, and then etched in an acetic-picric etchant (4.2 g picric acid, 10 ml water, 10 ml acetic acid and 70 ml ethanol) to reveal grain boundaries. Optical photomicrographs were obtained from the etched specimens using a Nikon EPIPHOT microscope equipped with a digital camera.

Electron Back Scattered Diffraction (EBSD)

For EBSD analysis, the annealed AZ31B alloy sheet was polished using a sequence of oil-based diamond suspensions of 9, 3, and 1 μm, respectively. This was followed by fine-polishing using colloidal silica. Finally, a 1 to 2 s etch using a solution of 60 ml ethanol, 20 ml distilled water, 15 ml acetic acid, and 5 ml nitric acid was applied. The EBSD data were collected in a Philips/FEI XL30 SEM at a voltage of 20 kV. A pole figure was calculated from the EBSD data using the MTEX open source toolbox for Matlab [17].

Results and Discussion

AZ31B alloy sheet was tested at 250 to 450°C at various gas-pressures, producing average true-strain rates measured near rupture to range from 10^{-3} to 10^{-1} s^{-1}. Three types of rupture were observed during these tests: (a) rupture along the RD, (b) rupture along the LTD, and (c) explosive rupture. Table II lists the rupture characters for both AZ31B under different testing conditions. The strain rates in Table II are given in ranges over which a particular rupture character was observed. From Table II, it can be concluded that, for temperatures from 350 to 450°C, AZ31B ruptured along the RD at slow rates ($\leq 3\times10^{-2}$ s^{-1}) and along the LTD at fast rates ($\geq 3\times10^{-2}$ s^{-1}). Multiple tests were conducted to evaluate the reproducibility of these rupture orientations. By changing the sheet orientation with respect to the die, it was confirmed that rupture direction was not caused by the orientation of the sheet in the dies.

Table II. The rupture characteristics of biaxial-bulge specimens are tabulated for different forming conditions

Temperature (°C)	Average true strain rate at pole (s^{-1})	Rupture orientation
450	10^{-3} to 3×10^{-2}	RD
	3×10^{-2} to 10^{-1}	LTD
350	10^{-3} to 3×10^{-2}	RD
	3×10^{-2} to 10^{-1}	LTD
300	10^{-3} to 2×10^{-2}	RD
	2×10^{-2} to 5×10^{-2}	Explosive
250	10^{-3} to 3×10^{-2}	Explosive

To investigate this rupture behavior, the biaxial-bulge specimens tested at 450°C and at strain rates of 10^{-3} s^{-1} and 10^{-1} s^{-1} were studied further. Explosive ruptures, as shown in Figure 3, prevented any such analysis of biaxial bulge specimens tested at 250 to 300°C. Figure 4 shows ruptured domes and photomicrographs of rupture cross-sections for these two specimens. The specimen tested at 10^{-3} s^{-1} ruptured primarily by cavitation, while the specimen tested at 10^{-1} s^{-1} ruptured primarily by necking. Grain-boundary-sliding (GBS) creep and dislocation-climb (DC) creep were identified as the dominant creep mechanisms, respectively, for the deformation of these specimens at 450°C [9].

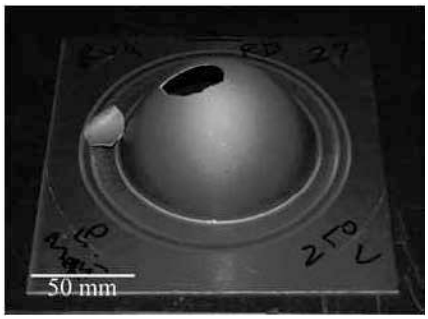

Figure 3. Explosive rupture in an AZ31B biaxial bulge specimen tested at 250°C and 2 × 10^{-3} s^{-1} is shown.

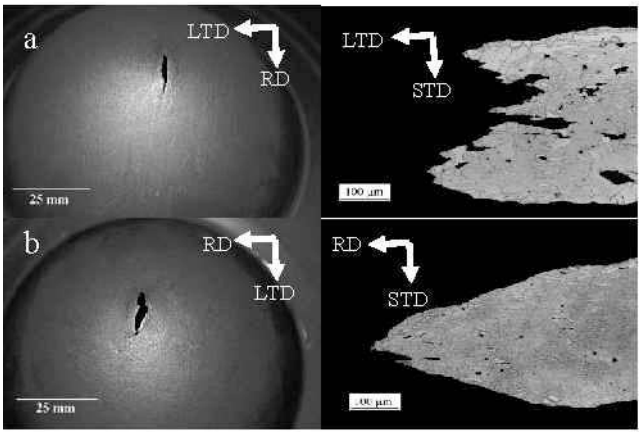

Figure 4. Ruptured domes and photomicrographs from the cross-sections of the ruptures are shown for AZ31B alloy sheet tested at 450°C and at (a) 10^{-3} s^{-1} and (b) 10^{-1} s^{-1}.

GBS creep dominates at slow strain rates, and DC creep dominates at the fast strain rates. Rupture by cavitation is consistent with deformation by GBS creep, which inhibits necking through a low stress exponent (approximately two) and promotes cavitation. Rupture by necking is consistent with deformation by DC creep, which is associated with a higher stress exponent (approximately 5). This high stress exponent provides less resistance to necking.

Rupture by cavity interlinkage is most likely to occur along the RD because the cavity nucleation sites, primarily second-phase particles and inclusions, tend to reside in stringers oriented along the RD. Thus, the biaxial bulge specimens failed by cavitation along the RD at slow strain rates ($\leq 3\times10^{-2}$ s^{-1}). The ruptures at fast strain rates occurred in necked regions. It is hypothesized that a small amount of planar anisotropy in the sheet leads to plane-strain necks aligned along the LTD at fast strain rates ($\geq 3\times10^{-2}$ s^{-1}). Although the planar anisotropy is not significant enough to affect the performance of material constitutive models that predict deformation [10], it might be sufficient to induce flow localization along a preferred direction.

Figure 5 shows stress-strain curves for three different specimen orientations, described as angle of the tensile axis from the sheet rolling direction (RD=0°, LTD=90° and 45°) in the AZ31B sheet at 450°C and at strain rates of 3×10^{-2} s^{-1} and 10^{-1} s^{-1}. These data are from tests previously analyzed in Ref [9]. The flow stress of the LTD (90°) specimens is slightly greater than that of the RD (0°) specimens. This indicates that the LTD is slightly stronger (harder) than the RD. The flow stress along the LTD is slightly higher than along the RD, necking will prefer deformation along the RD instead of the LTD, promoting plan-strain necking along a line parallel with the LTD (lowest-strain direction). This supports the hypothesis of planar anisotropy that affects flow localization.

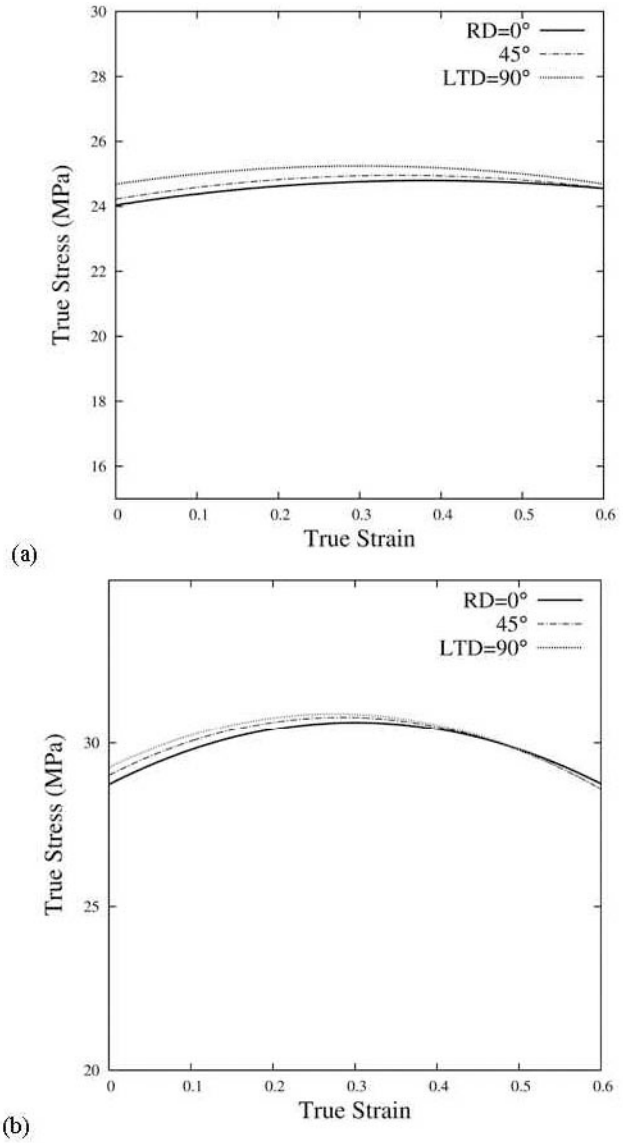

Figure 5. Stress-strain curves are shown for AZ31 alloy sheet at 450°C at (a) 3× 10^{-2} s^{-1} and (b) 10^{-1} s^{-1}. The orientation of the tensile direction with respect to the sheet rolling direction (RD) is specified in degrees (RD = 0°and LTD = 90°) [9].

The reason behind this anisotropy can be directly related to the crystallographic texture, as previously explained by Agnew *et al.* [18]. Figure 6 shows the <0001> pole figure obtained from AZ31B alloy sheet annealed and recrystallized at 450°C.

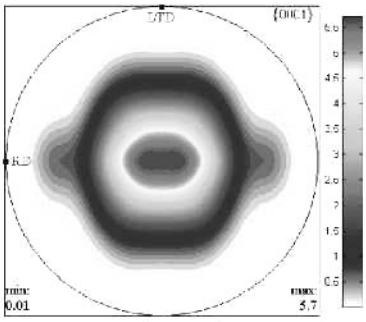

Figure 6. The <0001> pole figure of AZ31B alloy sheet annealed and recrystallized at 450°C for 30 minutes is shown.

Other than the basal fiber texture, the basal poles are spread slightly along the RD, which is consistent with the expected sheet texture noted in Ref [19]. This texture causes the LTD to be the harder in-plane direction and the RD to be the softer in-plane direction during deformation by slip, even though the difference may be slight. Dislocation-climb-controlled creep is the active deformation mechanism at the fast strain rates of interest ($\geq 3\times10^{-2}$ s^{-1}) at 450°C [9]. During the final stages of forming, deformation preferentially occurs along the RD, which causes plane-strain necking and the resulting rupture to be oriented along the LTD, as shown schematically in Figure 7.

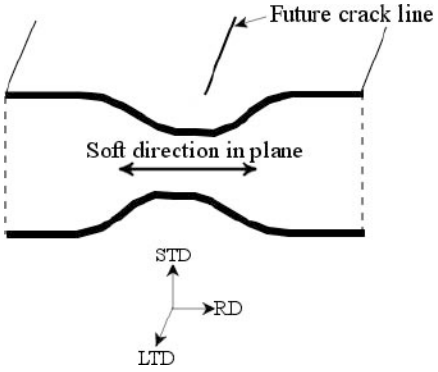

Figure 7. The effect of planar anisotropy on rupture orientation is shown. Deformation during necking occurs preferentially along the soft in-plane direction (the RD in AZ31B).

Similar texture [18], deformation [14] and rupture [13] mechanisms observed in AZ31B down to 350°C suggest that this hypothesis explains the rupture behavior from 350 to 450°C. The rupture orientation in AZ31B at 350 to 450°C helps identify the dominant rupture mechanism, among cavitation and necking, at a chosen strain rate.

Conclusions

Biaxial bulge testing was conducted for AZ31B alloy sheet at temperatures from 250 to 450°C. The rupture orientation at 350 to 450°C is controlled by the active mechanisms of plastic deformation. At slow strain rates ($\leq 3\times10^{-2}$ s^{-1}), cavity interlinkage associated with grain boundary sliding (GBS) creep is the dominant rupture mechanism, as shown in cross sections close to ruptures. This cavity interlinkage induces rupture along the rolling direction (RD). At fast strain rates ($\geq 3\times10^{-2}$ s^{-1}), flow localization (necking) associated with dislocation-climb (DC) creep is the dominant rupture mechanism. Planar anisotropy from the texture of the sheet causes necking to induce rupture along the long-transverse direction (LTD). This change in rupture orientation can be used as a method to identify the dominant rupture mechanism for AZ31B at a chosen strain rate and temperatures from 350 to 450°C. Explosive rupture prevented the analysis of AZ31B tested at 250 to 300°C.

References

1. A.A. Luo, "Magnesium: Current and Potential Automotive Applications," *JOM*, 54 (2002), pp. 42-48.

2. P.E. Krajewski, "Elevated Temperature Forming of Sheet Magnesium Alloys," *SAE Technical Paper*, (2001), Paper Number. 2001-01-3104.

3. L.H. Pomeroy, "Advantages of Lightweight Reciprocating Parts," *SAE Technical Paper,* (1922), Paper Number. 220044.

4. G.S. Cole, A.M. Sherman, "Light Weight Materials for Automotive Applications," *Material Characterization,* 35 (1995), pp. 3-9.

5. A.I. Taub, "Automotive Materials: Technology Trends and Challenges in 21st Century," *MRS Bulletin,* 31 (2006), pp. 336-34

6. A.I. Taub, P.E. Krajewski, A.A. Lou, J.N. Owens, "The Evolution of Technology for Materials Processing over the Last 50 Years: The Automotive Example," *JOM,* 59 (2007), pp. 48-57.

7. J.G. Schroth, "General Motors' Quick Plastic Forming Process," *Advances in Superplasticity and Superplastic Forming*, E.M. Taleff, P.A. Friedman, P.E. Krajewski, R.S. Mishra, and J.G. Schroth, eds., TMS, Warrendale, PA, 2004, pp. 9-20.

8. P.E. Krajewski, J.G. Schroth, "Overview of Quick Plastic Forming Technology," *Mat. Sci. Forum*, 2007, vol. 551-552, pp. 3-12.

9. P.A. Sherek, A.J. Carpenter, L.G. Hector, Jr., P.E. Krajewski, J.T. Carter, J. Lasceski, E.M. Taleff, "The Effects of Strain and Stress State in Hot Forming of Mg AZ31 Alloy Sheet," *Magnesium Technology*, S.M. Mathaudhu, W.H. Sillekens, N.R. Neelameggham , N.Hort, eds., TMS (2012), pp. 301-306.

10. G. Giuliano, S. Franchitti, "The Determination of Material Parameters from Superplastic Free-Bulging Tests at Constant Pressure," *International Journal of Machine Tools and Manufacture,* 48 (2008), pp. 1519-1522.

11. F. Abu-Farha, R. Verma, L.G. Hector Jr., "High Temperature Composite Forming Limit Diagrams of Four Magnesium AZ31B Sheets Obtained by Pneumatic Stretching," *Journal of Materials Processing Technology*, 212 (2012), pp. 1414-1429.

12. A.J. Carpenter, "Physics-Based Material Constitutive Models for the Simulation of High-Temperature Forming of

Magnesium Alloy AZ31," PhD Thesis, University of Texas at Austin, (2012).

13. E. Hsu, J. Szpunar, R. Verma, "Effect of Temperature and Strain Rate on Formability of AZ31 Magnesium Sheet alloy," *SAE Technical Paper*, (2006), Paper Number. 2006-01-0258.

14. E.M. Taleff, L.G. Hector, Jr., R. Verma, P.E. Krajewski, J.K. Chang, "Material Models for Simulation of Superplastic Mg Alloy Sheet Forming," *Journal of Materials Engineering and Performance,* 9 (2010), pp. 488-494.

15. Yin D.L., "Superplasticity and cavitation in AZ31 Mg Alloy at elevated temperatures," *Materials Letters*, 59 (2005), pp. 1714-1718.

16. ASM International, *Metals Handbook. Vol. 2: Properties and Selection: Nonferrous Alloys and Pure Metals*, (Materials Park, OH, 2002).

17. F. Bachmann, R. Hielscher, H. Schaeben, "Texture Analysis with MTEX – Free and Open Source Software Toolbox," *Solid State Phenomena*, 160 (2010), pp. 63-68.

18. S.R. Agnew, O. Duygulu, "Plastic Anisotropy and the Role of Non-basal Slip in Magnesium Alloy AZ31B," *International Journal of Plasticity*, (2005), pp. 1161-1193.

19. U.F. Kocks, C.N. Tome, H.-R. Wenk (Eds.), *Texture and Anisotropy: Preferred Orientations in Polycrystals and their Effect on Materials Properties,* (Cambridge, New York 2000), pp. 204-206.